

Article

A Novel Fast Contact Operating Mechanism of the Medium and Low Voltage Hybrid DC Current Limiting Circuit Breaker

Zhiyong Lv¹, Xiangjun Wang¹, Jinwu Zhuang¹, Zhuangxian Jiang², Zhifang Yuan³, Luhui Liu³ and Jin Wu^{1,*}¹ College of Electrical Engineering, Naval University of Engineering, Wuhan 430033, China² College of Electrical Engineering, Zhejiang University, Hangzhou 310058, China³ National Key Laboratory of Science and Technology on Vessel Integrated Power System, Naval University of Engineering, Wuhan 430033, China

* Correspondence: wujin.lj@163.com

Abstract: In order to solve the problem of the slow initial speed caused by the large mass of the bistable permanent magnetic actuator (PMA) in the traditional bistable permanent magnetic–electromagnetic repulsion mechanism (PM-ERM), a novel fast contact operating mechanism is proposed by using the flexible spring system (SS) between the PMA and the ERM. The novel structure can separate the mass of the PMA and the ERM at the initial phase of the interrupting process, improve the initial speed of the contact and increase the initial opening distance of the contact. Firstly, the paper conducts an extensive investigation and analysis of the principle of the existing fast operating mechanism and points out the advantages and disadvantages of the existing mechanism. In order to meet the requirement of fast interrupting and improve the service life of the mechanism, a novel mechanism is proposed. And then, the working principle of the novel mechanism is introduced. The cooperative relationship between the ERM and the PMA and the working principle and performance parameter requirements of the ERM, SS and PMA are analyzed and designed. Finally, the feasibility of the novel mechanism is verified by the experiment. The results show that the opening distance of the novel operating mechanism can reach 2.25 mm in 1 ms. Compared with 1.24 mm of the traditional operating mechanism, it improves the initial opening distance of the contact by 81.5% and is conducive to the rapid interruption of the Hybrid DC current-limiting circuit breaker (HDCCLCB).

Keywords: HDCCLCB; PM-ERM; SS; ERM; PMA; initial speed

Citation: Lv, Z.; Wang, X.; Zhuang, J.; Jiang, Z.; Yuan, Z.; Liu, L.; Wu, J. A Novel Fast Contact Operating Mechanism of the Medium and Low Voltage Hybrid DC Current Limiting Circuit Breaker. *Electronics* **2024**, *13*, 4270. <https://doi.org/10.3390/electronics13214270>

Academic Editor: Spyridon Nikolaidis

Received: 13 June 2023

Revised: 14 November 2023

Accepted: 28 November 2023

Published: 31 October 2024



Copyright: © 2024 by the authors. Licensee MDPI, Basel, Switzerland. This article is an open access article distributed under the terms and conditions of the Creative Commons Attribution (CC BY) license (<https://creativecommons.org/licenses/by/4.0/>).

1. Introduction

The ship-integrated power system (IPS) combines the mechanical propulsion and electric power systems in the traditional ship, supplies power to propulsion, weapons, communication, navigation and daily equipment in the form of electric energy, and realizes the comprehensive utilization of energy in the whole ship. It is known as the third revolution of ship power [1,2]. The typical characteristics of the ship's DC power system are low line impedance, a small time constant, a high short-circuit current rise rate, and a high expected short-circuit current peak value, which create high requirements for the rapidity of the DC circuit breaker [3–6]. The action time of a traditional mechanical circuit breaker is generally at the millisecond level [7], which makes it difficult to meet the requirements. Solid state circuit breakers have the disadvantage of a large rated current loss and need additional heat dissipation devices [8–10].

HDCCLCB combines the characteristics of large capacity and low loss of mechanical switch with the rapidity of a solid-state switch. It has become an effective way to solve the problem of large capacity and fast DC interruption [11,12]. The speed of the mechanical switch in the HDCCLCB is an important factor affecting its rapidity [13,14].

The operating mechanism of a fast mechanical switch in the medium- and low-voltage current-limiting circuit breaker generally has the following schemes [15–22]: (1) The ERM +

bistable butterfly spring/bistable spring: This scheme uses the elastic force of the bistable butterfly spring/bistable spring at the opening and closing positions to provide holding force, and respectively adopts a set of ERM to drive during opening and closing action processes [15,16]. (2) The ERM + pawl+ compression spring: This scheme uses springs to provide the maintaining force at the closing state, the ERM realizes rapid opening of the contact, and the pawl keeps the contact open [17,18]. (3) The ERM + compression spring + monostable PMA: This scheme uses the monostable PMA to provide the maintaining force at the closing state. The ERM realizes rapid opening of the contact and the spring provides the maintaining force at the opening state [19,20]. Due to the use of ERM to simultaneously handle normal, overload, and short circuit situations in schemes (1)~(3), the service life of the mechanical switch cannot be guaranteed. Therefore, scheme (4) is proposed. Scheme (4) is bistable PMA + ERM: This scheme utilizes the advantages of fewer parts, simple structure and the high reliability of the PMA to realize the action under rated load conditions and below, so as to reduce the frequent actions of ERM and improve the service life of the circuit breaker. When overload and short circuit faults occur, the ERM and the PMA act simultaneously [21,22]. In scheme (4), the normal, overload and short circuit conditions are treated separately, but the mass of the moving iron core of the PMA is large, which will lead to an extension of the inherent opening time of the mechanical switch and a slower initial speed.

In order to solve the problem of the slow initial speed of the traditional PM-ERM, this paper proposes a new type of PM-ERM with a flexible connection for the first time. The new mechanism can separate the mass of moving components during the initial movement of the contact, improve the initial speed and increase the initial opening distance of the contact, which is conducive to improving the breaking capacity of the fast DC circuit breaker. And the feasibility of the new operating mechanism has been verified through experiments.

2. Structure and Working Principle of the Novel Fast Contact Operating Mechanism

The novel fast contact operating mechanism is mainly composed of the bistable PMA, SS and ERM. Its structural diagram is shown in Figure 1.

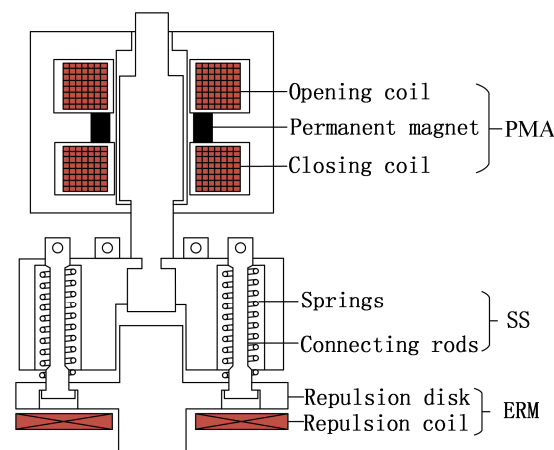


Figure 1. Structural diagram of the novel fast contact operating mechanism.

The PMA not only completes the opening action of the system under normal operating conditions but also completes the closing action under all working conditions. When an overload or short-circuit fault occurs, in order to quickly limit the short-circuit current, the ERM and the PMA are jointly driven to complete the opening action. The ERM is used to quickly establish the initial distance, and then the PMA is used to maintain the opening state. The SS realizes the flexible connection between the PMA and the ERM, so that in the case of a short-circuit fault, the PMA and the ERM are separated in mass, and the contact can obtain a higher initial speed and a greater opening distance in a short time, which improves the interrupting capability of the HDCCLCB.

Different from the traditional BPM-ERM, the PMA and the ERM in the novel operating mechanism are not directly driven by a connecting rod, but a spring system is used to achieve a flexible connection, as shown in Figure 2.

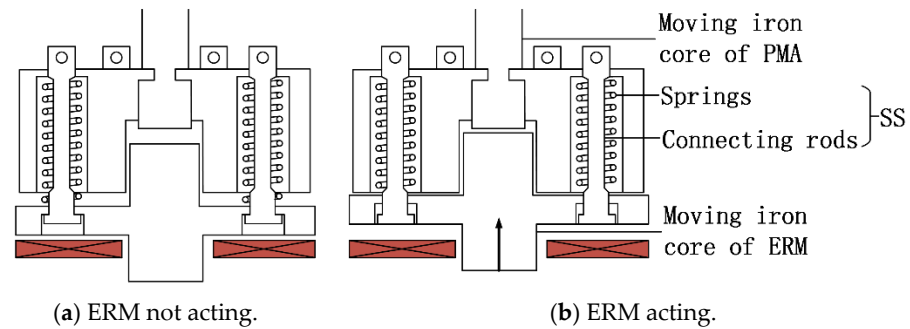


Figure 2. Structural diagram of the SS.

The SS consists of multiple springs, connecting rods and slots. Initially, the spring is compressed to produce a downward force on the repulsion disk, and the closing pressure F_0 to the contact. Because the mechanical switch needs to ensure that no welding occurs when the contact flows through a large current under certain special working conditions, it is necessary to provide sufficient closing pressure. The initial pressure is given here as 1600 N. The force of the spring on the repulsion disk will make the repulsion disk move downward. In order to limit the distance between the repulsion disk and the PMA, the slots on the connecting rods are used to limit the downward movement of the repulsion disk relative to the PMA. Therefore, the distance between the two will not be greater than the initial opening distance. As shown in Figure 2b, when the ERM acts, the moving iron core of ERM moves upwards, while the moving iron core of PMA does not act, which will cause the springs to be compressed. Subsequently, the PMA begins to act after a period of inherent time, and gradually, the displacement of the PMA becomes equal to the displacement of the ERM. Afterwards, the ERM and PMA act together. Before the displacement of the two is the same, the mass of the moving components of the ERM and the PMA is separated.

The following is an analysis of the action process of the novel mechanism in the case of a short-circuit fault in the system. Figure 3 shows the displacement curves of the ERM and PMA.

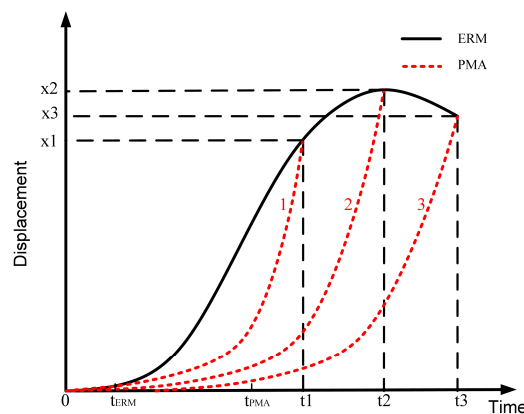


Figure 3. Displacement curves of the ERM and PMA.

At zero time, the ERM and PMA are triggered. After a phase of delay, at time t_{ERM} , the ERM starts to open and obtains a large initial speed. Since the inherent time of the PMA is longer than that of the ERM, the PMA does not open, the spring is continuously compressed and the ERM decelerates under the force of the SS. At the time t_{PMA} , the PMA starts to move. If the distance between the ERM and SS is not sufficient, the ERM will

directly hit the SS. The direct hit will cause the speed of the ERM to drop, which slows down the speed of the contact in the initial phase of the interrupting process, so it is not considered. There are three situations according to the speed relationship between the ERM and PMA when their displacements are equal, as shown by the dotted line in Figure 3. The dotted lines 1 and 2 have high requirements for the speed of the PMA, which will lead to large energy consumption and volume of the driving power supply. Therefore, the displacement characteristics displayed by dotted line 3 are finally selected for the scheme design.

3. Analysis and Design of the Novel Fast Contact Operating Mechanism

This section will provide corresponding design requirements for each part of the fast-operating mechanism according to the results of the above analysis. Each part is analyzed and designed by means of analysis and numerical simulation.

3.1. Analysis and Design of the ERM

The high-speed ERM is mainly composed of three parts: a pulse discharge circuit, a repulsion coil and a repulsion disk. Figure 4 shows the schematic diagram of a high-speed ERM, in which C_1 is the discharge capacitor, TH_1 is the power thyristor and D_1 is the diode. When TH_1 receives a turn-on signal, capacitor C_1 immediately discharges. The repulsion coil forms a pulse current and generates a pulse magnetic field around the repulsion coil. The repulsion disk above the repulsion coil generates an induced current under the changing pulse magnetic field. A huge electromagnetic repulsion force is generated between the repulsion coil and the repulsion disk to realize the rapid drive of the repulsion disk.

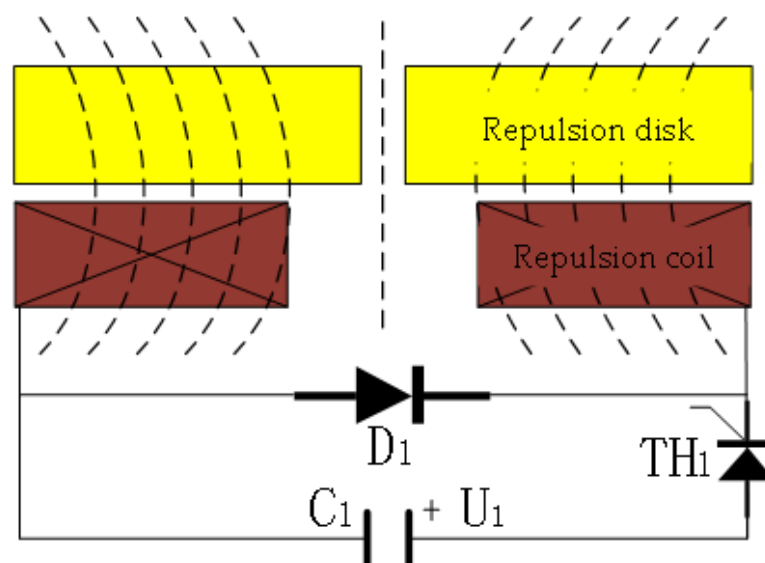


Figure 4. Schematic diagram of the ERM.

The ERM mainly completes the rapid interruption in the case of overload and short-circuit faults. It is required to obtain a large opening distance at the initial phase of the interrupting process; the opening distance within 1 ms shall reach 2 mm.

The repulsion disk is equivalent to a group of closed coils, and its winding direction is the same as that of the repulsion coil. Figure 5 shows the equivalent circuit of the ERM, where i_1 represents the repulsion coil current and i_2 represents the induced current in the equivalent repulsion disk coil.

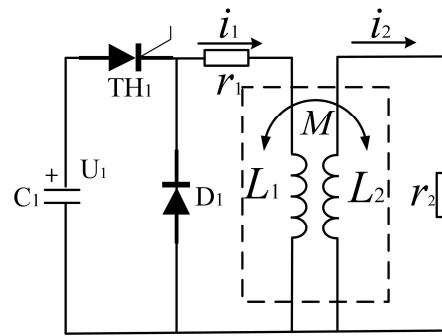


Figure 5. Equivalent circuit diagram of the ERM.

The research results in reference [19] show that when the speed and opening distance of the repulsion disk are small, the change of mutual inductance with time dM/dt can be considered a constant and the mutual inductance M can be considered a fixed value. The mathematical equation of ERM can be obtained:

$$\begin{cases} U_1 = i_1 r_1 + L_1 \frac{di_1}{dt} - M \frac{di_2}{dt} \\ M \frac{di_1}{dt} = i_2 r_2 + L_2 \frac{di_2}{dt} \\ i_1 = -C \frac{dU_1}{dt} \\ F_m = -\frac{dM}{dx} i_1 i_2 \\ m \frac{d^2 x}{dt^2} = F_m \end{cases} \quad (1)$$

Since the equivalent coil parameters of the repulsion disk in Formula (1) are difficult to accurately obtain, the finite element numerical calculation method is used to analyze the motion characteristics and establish a two-dimensional axisymmetric finite element simulation model, as shown in Figure 6.

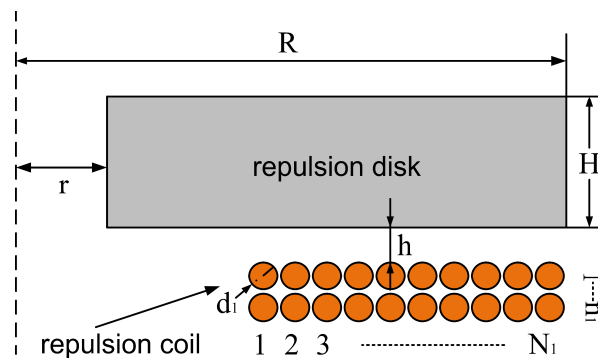


Figure 6. Geometric diagram of the ERM.

We used the finite element numerical simulation calculation method to analyze the influence of the electric gap h , number of single-layer coil turns N_1 , number of coil layers n_1 and the capacitor voltage U_1 on the motion characteristics of the ERM. The analysis process does not consider the influence of the displacement of the PMA.

The curve of the electromagnetic repulsion force and displacement with time under different electric gaps is shown in Figure 7. It can be seen from Figure 7 that, with the increase in the electrical gap, the displacement of the ERM decreases. This is because with the increase in the electrical gap, the magnetic coupling between the repulsion coil and the repulsion disk decreases, which leads to a decrease in the induced current and the rate of change of mutual inductance between the coil and the repulsion disk with respect to displacement, making the electromagnetic repulsion force smaller, so the displacement of the ERM also becomes smaller.

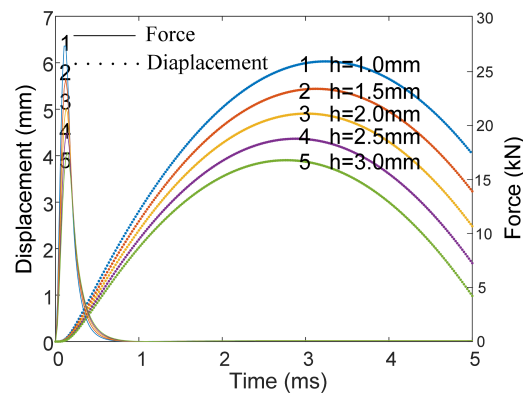


Figure 7. Curves of the electromagnetic repulsion force and displacement with time under different electric gaps.

When the outer diameter of the ERM is certain, the influence of the number of turns N_1 on the displacement of the ERM is analyzed and the results are shown in Figure 8. It can be seen from Figure 8 that the displacement of the ERM increases with the increasing number of turns. This is because with the increase in the number of turns, the forcing area of the ERM increases, and the peak value of the electromagnetic repulsion force increases, so the displacement of the ERM increases.

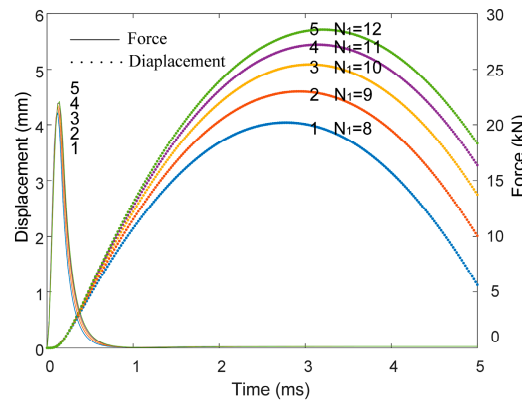


Figure 8. Curves of the electromagnetic repulsion force and displacement with time under different coil turns.

Considering the influence of different coil layers n_1 on the displacement, the results are shown in Figure 9.

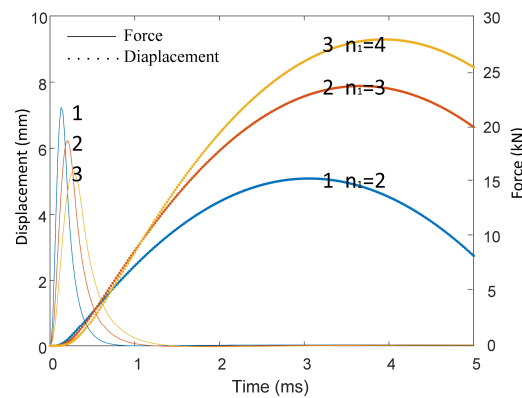


Figure 9. Curves of the electromagnetic repulsion force and displacement with time under different coil layers.

With the increase in the coil layers, the displacement of the ERM increases. This is because with the increase in coil layers, the peak value of the electromagnetic repulsion force is delayed. Although the peak value becomes smaller, the attenuation of electromagnetic repulsion force becomes slower. The displacement of the ERM is mainly affected by the duration of the electromagnetic repulsion force.

When the energy provided by the capacitor is constant, the influence of voltage change on the displacement is considered, and the results are shown in Figure 10. With the increase in capacitor voltage, the peak value of electromagnetic repulsion force decreases, and the displacement of ERM is mainly affected by the peak value of electromagnetic repulsion force.

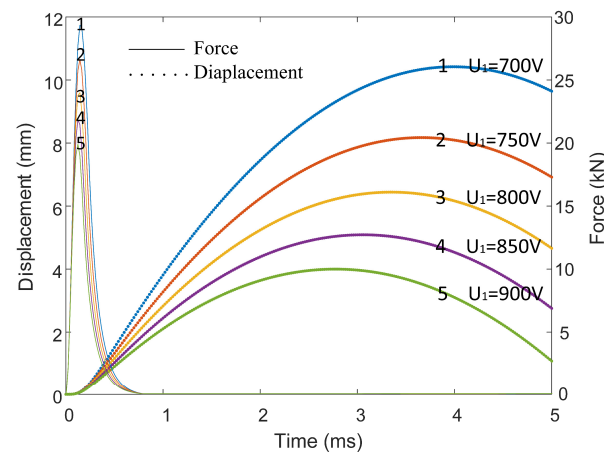


Figure 10. Curves of the electromagnetic repulsion force and displacement with time under different voltages.

It can be seen from the calculation results of Figures 7–10 that the electromagnetic repulsion force generally decays completely within 1 ms, and the external force has an influence on the movement characteristics of the mechanism after 1 ms. Before the displacement of the ERM is equal to that of the PMA, the spring pressure on the ERM will change with the increase in displacement. If the spring stiffness coefficient is too large, the external force on the ERM will be too large and the displacement will be small.

3.2. Analysis and Design of the SS

The spring system compresses multiple springs in parallel and evenly arranges them on the upper surface of the repulsive disk, which generates a downward force on the upper surface of the repulsive disk. Limiting the downward movement of the repulsive disk is realized through the cooperation of the connecting rods and the slots while maintaining the compressed state to provide the initial pressure of the contact.

In order to ensure the uniform force of the repulsive disk, six springs are used to evenly distribute the initial pressure of 1600 N. At the same time, it is necessary to ensure that the compression pressure within 6 mm does not change more than 30%, so the single stiffness coefficient is 13 N/mm.

3.3. Analysis and Design of the PMA

The bi-stable PMA is mainly composed of a static iron core, a moving iron core, an opening coil, a closing coil and a permanent magnet. The schematic diagram of the structure is shown in Figure 11.

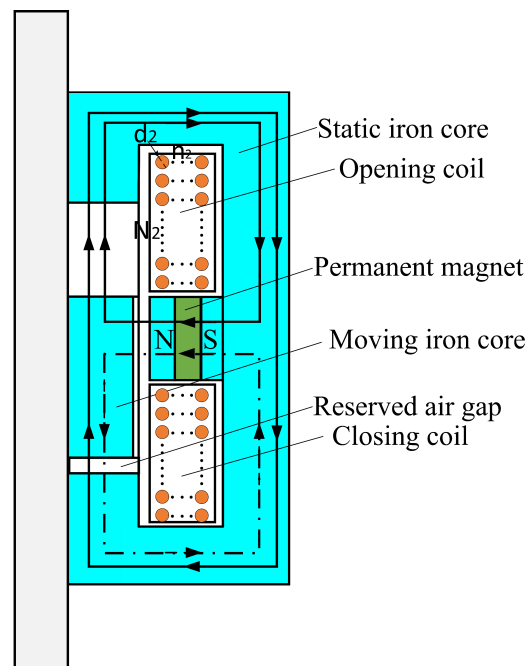


Figure 11. Structural diagram of the bistable PMA.

In Figure 11, the bi-stable PMA is in the closed state, and most of the magnetic flux generated by the permanent magnet circulates through the path shown by the dotted line, generating a downward electromagnetic force F_1 to the moving iron core [17]:

$$F_1 = \frac{B_1^2}{2\mu_0} S_1 \quad (2)$$

where B_1 is the magnetic flux density at the reserved air gap, μ_0 is the vacuum permeability and S_1 is the area of the lower surface of the moving iron core.

At the opening action, the magnetic flux generated by the current of the opening coil passes through the path shown by the solid line. On the one hand, it will increase the air gap magnetic flux density on the upper surface of the moving iron core. On the other hand, it will partially offset the magnetic flux density on the lower surface of the moving iron core generated by the permanent magnet. When the current increases to a certain extent, it will move upward to begin opening. The closing action process is the opposite.

Under the overload and short circuit conditions of the system, the PMA needs to act quickly together with the ERM, and the PMA is required to reach the opening distance of 4 mm within 4 ms. In the early phase of the opening process, the moving iron core is not only affected by the electromagnetic force generated by the opening coil and permanent magnet but also affected by the upward force from the SS (the force is temporarily considered to be constant, without considering the influence of displacement of the repulsion mechanism).

We established the finite element numerical calculation model shown in Figure 11 to analyze the parameters that affect its movement characteristics. As shown in Figure 12, the electromagnetic force and displacement curves of PMA under different coil layers n_2 are shown; it can be seen from the figure that with the increase in coil layers, the rising speed of the electromagnetic force gradually slows down, but the amplitude of electromagnetic repulsion force gradually increases, and the displacement of the PMA, which is mainly affected by the rising speed of electromagnetic force, gradually decreases.

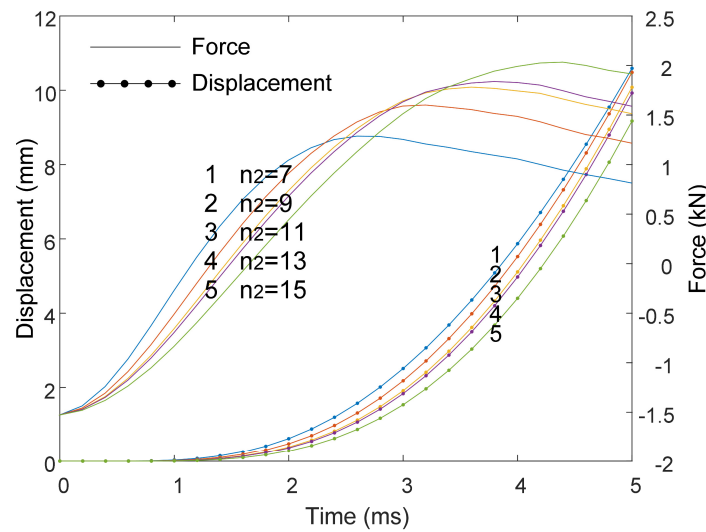


Figure 12. Curves of the electromagnetic force and displacement with time under different coil layers.

When the area occupied by the coil cross section is certain, the electromagnetic force and displacement curves of the PMA under different wire diameters d_2 are shown in Figure 13. It can be seen from Figure 13 that as the wire diameter increases, the number of coil turns N_2 and coil layers n_2 decreases, the electromagnetic force rises faster and the electromagnetic force amplitude becomes smaller. The displacement of the PMA is mainly affected by the electromagnetic force’s rising speed and thus gradually increases.

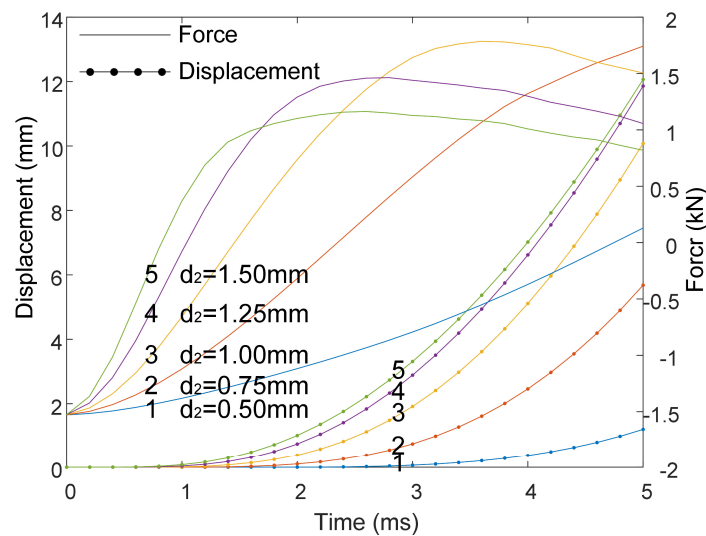


Figure 13. Curves of the electromagnetic force and displacement with time under different wire diameters.

In the case of keeping the capacitor energy constant, the electromagnetic force and displacement curves of the PMA under different capacitor voltages are shown in Figure 14. It can be seen from Figure 14 that as the voltage increases, the capacitance decreases, the current rising speed becomes faster and the current amplitude becomes smaller, so the electromagnetic force rises faster, and the amplitude of the electromagnetic force becomes smaller. The displacement of the PMA is mainly affected by the electromagnetic force’s rising speed and thus becomes larger.

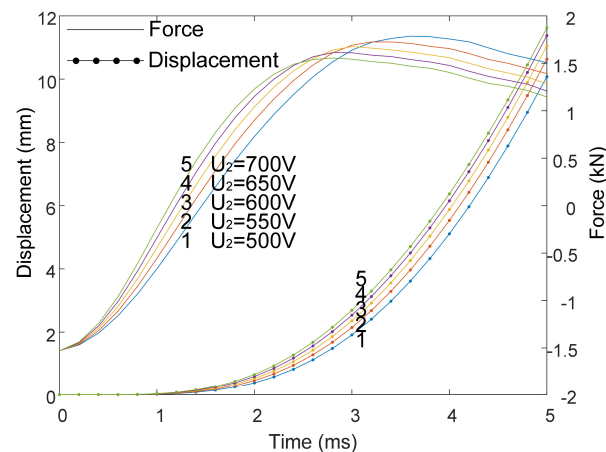


Figure 14. Curves of the electromagnetic force and displacement with time under different voltages.

From the calculation results of Figures 12–14, it can be seen that displacement of the PMA within 4 ms is mainly affected by the rising speed of the electromagnetic force. The faster the rising speed, the greater the displacement of the PMA in a short time.

4. Experiment Verification

To ensure the reliable closing of the circuit breaker, the contact opening distance should be large enough before the end of the zero-voltage time. The ERM has become the first choice of driving mechanisms because of its short inherent time and large initial speed. Under the condition of ensuring that the ERM will not be damaged, and the requirements of the small energy consumption and small overall volume of the mechanism are met at the same time, the movable contact displacement should reach its maximum at 500 μ s.

Based on the above analysis and combined with the actual engineering, the parameters are reasonably selected to manufacture the prototype and the experimental platform is built to verify the novel fast contact operating mechanism scheme. The SS realizes the flexible connection between the ERM and the bi-stable PMA. The physical diagram of the SS is shown in Figure 15.



Figure 15. Physical picture of the SS.

The experiments of the ERM acting alone, PMA acting alone and the combined action of the two have been completed successively to verify the design results of each part of the mechanism, respectively. The schematic diagram of the experimental platform is shown in Figure 16. At the zero time, the TH₁ and TH₂ thyristors were triggered in different situations, and the Photron SA4 high-speed camera was used to take pictures of the lower end of the connecting rod (the speed at this position is considered to be the same as the contact speed). The shooting speed is 50,000 fps and the resolution is 192 \times 128. Figure 17 shows the experimental site.

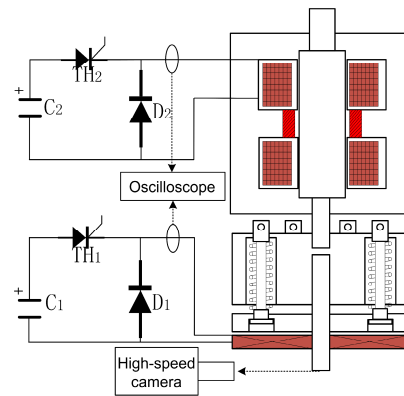


Figure 16. Schematic diagram of the experimental platform.

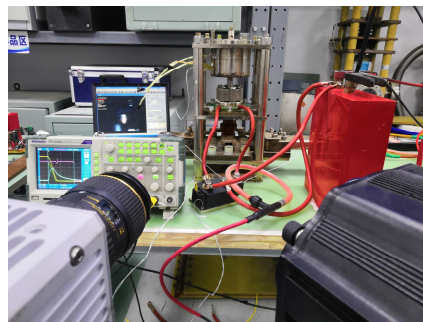


Figure 17. Experimental site.

Figures 18–20 show the contact displacement comparison diagrams of the experimental and simulation of the ERM acting alone, the PMA acting alone and both acting jointly.

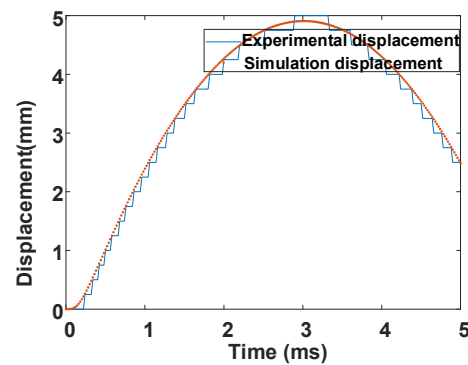


Figure 18. The displacement curve of the contact when the ERM acts alone.

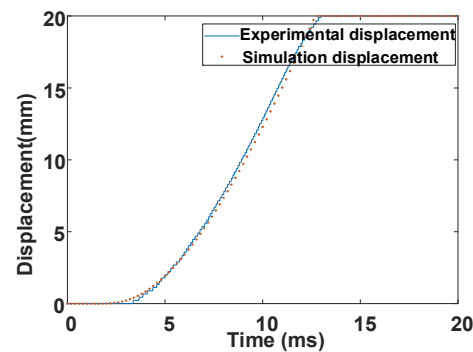


Figure 19. The displacement curve of the contact when the PMA acts alone.

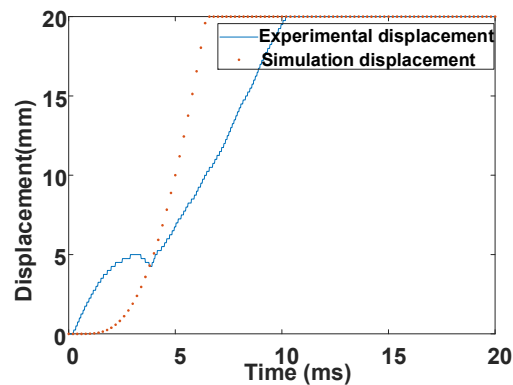


Figure 20. The displacement curve of the contact in joint action.

In Figure 18, due to the closing force of 1600 N of the PMA, it can be seen that when the ERM acts alone, the displacement of the PMA is zero. The pressure of the SS on the ERM changes linearly with the displacement. The results show that the displacement of the contact is 2.25 mm at 1 ms and 4.25 mm at 4 ms. The relative error between simulation and experiment is small.

In Figure 19, when the PMA acts alone, due to the connection of the SS, the electromagnetic force generated by the PMA drives the PMA and the ERM to move at the same time. It can be seen from the results that the relative error between simulation and experiment is small.

The dotted line in Figure 20 is the simulation displacement curve under the initial elastic force of the SS when the PMA acts alone without considering the mass of the ERM. The solid line represents the displacement curve of the contact in joint action. It can be seen from Figure 20 that in the case of joint action, the contact will experience a short delay under the action of the ERM to obtain a large initial speed. The opening distance of 1 ms will reach 2.25 mm, and then the speed will gradually decrease under the pressure of the spring system until it reverses.

At 4 ms, the speed suddenly changes and the displacement of the PMA and the ERM is the same as 4.25 mm. Then, they move to the opening position synchronously. The contact speed suddenly changes at 4 ms, and the solid line intersects the dotted line (the dotted line is the simulation displacement curve under the initial elastic force of the SS when the PMA acts alone and does not consider the mass of the ERM). Therefore, it can be considered that the thrust of the SS has a small impact on the movement of the PMA. At the same time, it can be concluded that the error between the displacement of simulation results of the PMA and the experimental displacement is small, which verifies the accuracy of the simulation model.

The displacement characteristics of contact are simulated by a finite element method under the condition of a traditional direct drive connection method (the mass of moving parts is the same as that of the novel operating mechanism). The dotted line in Figure 21 represents the displacement characteristics of the operating mechanism in the traditional connection method, and the solid line is the displacement curve of the novel operating mechanism. Compared with the opening distance of 1.24 mm at 1 ms under the traditional connection method, the novel operating mechanism can obtain a larger opening distance of 2.25 mm due to the mass separation at the initial phase of the interrupting process, and the end speed of the new mechanism is also lower than that of traditional mechanisms. Overall, compared with traditional mechanisms, the new mechanism exhibits the characteristics of a fast initial speed and a slow end speed, which is conducive to improving the interrupting capacity of the HDCCLCB.

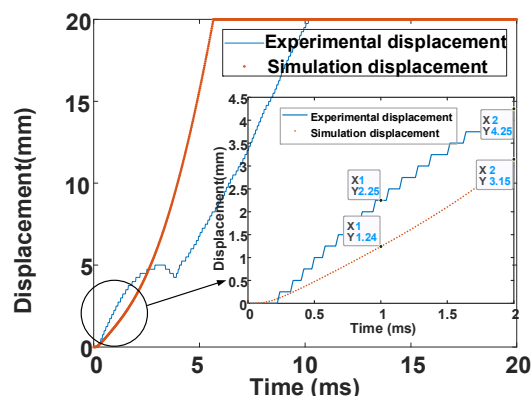


Figure 21. The displacement curve of the novel contact operating mechanism and traditional contact operating mechanism.

5. Conclusions

In order to meet the practical needs of fast current limiting protection in medium- and low-voltage DC power systems, a novel structure for the fast contact operating mechanism is proposed by investigating the existing fast contact operating mechanism. Compared with traditional mechanisms, the novel structure exhibits characteristics of a fast initial speed and a slow end speed, which can increase the initial opening distance while reducing the impact at the end. The research results can be applied to such occasions as microgrids, rail transit, electric aircraft, distributed power generation, ship power systems and so on, which provides a new idea for rapid protection of DC power systems.

Author Contributions: Conceptualization, Z.L., X.W., J.Z. and J.W.; methodology, Z.L.; software, Z.L.; investigation, L.L. and Z.Y.; writing—original draft preparation, Z.L.; writing—review and editing, Z.L.; project administration, Z.J.; funding acquisition, L.L. and Z.Y. All authors have read and agreed to the published version of the manuscript.

Funding: This research was funded by [National Natural Science Foundation of China] grant number [52107136, 51607184].

Data Availability Statement: The data presented in this study are available on request from the corresponding author. The data are not publicly available due to [confidentiality requirements of the school].

Conflicts of Interest: The authors declare no conflict of interest.

References

1. Ma, W.M. The Integrated Power System in Warship. In Proceedings of the 5th International Marine Electrotechnology Conference, Shanghai, China; 2003; Volume 1, pp. 2–7.
2. Ma, W.M. Integrated Power Systems—Trend of Ship Power Development. *J. Nav. Univ. Eng.* **2002**, *14*, 1–6.
3. Chen, H. DC-ZEDS based shipboard integrated power system. *Ship Sci. Technol.* **2005**, *27*, 31–37. (In Chinese)
4. Fu, L.; Chen, B.; Ye, Z. Short-circuit current calculation for DC meshy network. *High Volt. Eng.* **2008**, *34*, 1731–1736. (In Chinese)
5. Franck, C.M. HVDC circuit breakers: A review identifying future research needs. *IEEE Trans. Power Deliv.* **2011**, *26*, 998–1007. [[CrossRef](#)]
6. Wen, W.; Huang, Y.; Al-Dweikat, M.; Zhang, Z.A.; Cheng, T.; Gao, S.; Liu, W. Research on operating mechanism for ultra-fast 40.5-kV vacuum switches. *IEEE Trans. Power Deliv.* **2015**, *30*, 2553–2560. [[CrossRef](#)]
7. Desbaillet, M. *DC High Speed Circuit-Breaker UR6 Instructions Manual Document Number: HSBA601103TEN*; Secheron SA: Geneva, Switzerland, 2008.
8. Xu, Z.; Zhang, B.; Sirisukprasert, S.; Zhou, X.; Huang, A.Q. The emitter turn-off thyristor-based DC circuit breaker. In Proceedings of the 2002 IEEE Power Engineering Society Winter Meeting, New York, NY, USA, 27–31 January 2002; Volume 1, pp. 288–293.
9. Agostini, F.; Vemulapati, U.; Torresin, D.; Arnold, M.; Rahimo, M.; Antoniazzi, A.; Raciti, L.; Pessina, D.; Suryanarayana, H. 1MW bi-directional DC solid state circuit breaker based on air cooled re-verse blocking-IGCT. In Proceedings of the 2015 Electric Ship Technologies Symposium, Old Town Alexandria, VA, USA, 21–24 June 2015; pp. 287–292.
10. Kempkes, M.; Roth, I.; Gaudreau, M. Solid-state circuit breakers for medium voltage DC power. In Proceedings of the 2011 Electric Ship Technologies Symposium, Alexandria, VA, USA, 10–13 April 2011; pp. 254–257.

11. Steurer, M.; Frolich, K.; Halaus, W.; Kaltenecker, K. A novel hybrid current-limiting circuit breaker for medium voltage: Principle and test results. *IEEE Power Eng. Rev.* **2002**, *22*, 62. [[CrossRef](#)]
12. Häfner, J.; Jacobson, B. Proactive hybrid HVDC breakers—A key innovation for reliable HVDC grids. In Proceedings of the Cigré Bologna (International Council on Large Electric Systems); 2011; p. 264.
13. Yamaguchi, S.; Sasao, H.; Hasegawa, H.; Ikeda, K.; Tukamoto, T. Mechanical arcless dc circuit breaker by current zero operation. *Rev. Sci. Instrum.* **1992**, *63*, 3993–3999. [[CrossRef](#)]
14. Zyborski, J.; Lipski, T.; Czucha, J.; Hasan, S. Hybrid arcless low-voltage AC/DC current limiting interrupting device. *IEEE Trans. Power Deliv.* **2000**, *15*, 1182–1187. [[CrossRef](#)]
15. Yuan, Z.; He, J.; Pan, Y.; Jing, X.; Zhong, C.; Zhang, N.; Wei, X.; Tang, G. Research on ultra-fast vacuum mechanical switch driven by repulsive force actuator. *Rev. Sci. Instrum.* **2016**, *87*, 125103. [[CrossRef](#)] [[PubMed](#)]
16. Vilchis-Rodriguez, D.S.; Shuttleworth, R.; Smith, A.C.; Barnes, M. Design, Construction, and Test of a Lightweight Thomson Coil Actuator for Medium-Voltage Vacuum Switch Operation. *IEEE Trans. Energy Convers.* **2019**, *34*, 1542–1552. [[CrossRef](#)]
17. Roodenburg, B.; Kaanders, M.A.M.; Huijser, T. First results from an electro-magnetic (EM) drive high acceleration of a circuit breaker contact for a hybrid switch. In Proceedings of the 11th European Conference on Power Electronics and Applications, Dresden, Germany, 11–14 September 2005; pp. 1–10, ISBN 90-75815-08-5.
18. Roodenburg, B.; Evenblij, B.H.; Huijser, T. Simulation of a flat spiral inductor-disk geometry for electro-magnetic (EM) acceleration. In Proceedings of the 2nd European Pulsed Power Symposium, DESY, Hamburg, Germany, 20–23 September 2004; Shaker Verlag: Aachen, Germany, 2004; pp. 202–206, ISBN 3-8322-3217-6.
19. Liang, D.; Dong, W.; Zhang, S.; Zou, J.; Wang, Y.; Wang, Z. Investigations on Electromagnetic Operating Mechanism of DC Vacuum Circuit Breaker. In Proceedings of the 2018 IEEE 3rd Advanced Information Technology, Electronic and Automation Control Conference (IAEAC), Chongqing, China, 12–14 October 2018; pp. 1349–1352.
20. Hou, Y.; Shi, Z.; Li, S.; Yao, Q.; Miao, Y.; Zhang, S.; Qiu, N. Research on Fast Opening Process in Electromagnetic Repulsion Mechanism. *IEEE Trans. Magn.* **2019**, *55*, 8000704. [[CrossRef](#)]
21. Li, Y.; Xia, K.; Liu, W.; Li, D. Design and simulation analysis of electromagnetic repulsion mechanism. In Proceedings of the 2010 IEEE International Conference on Industrial Technology, Via del Mar, Chile, 14–17 March 2010; pp. 914–918.
22. Zhang, M.; Wang, Y.; Li, P.; Wen, H. Comparative Studies on Two Electromagnetic Repulsion Mechanisms (ERMs) for High Speed Vacuum Switch. *IET Electr. Power Appl.* **2017**, *12*, 247–253. [[CrossRef](#)]

Disclaimer/Publisher’s Note: The statements, opinions and data contained in all publications are solely those of the individual author(s) and contributor(s) and not of MDPI and/or the editor(s). MDPI and/or the editor(s) disclaim responsibility for any injury to people or property resulting from any ideas, methods, instructions or products referred to in the content.